Int. J. Electrochem. Sci., 15 **(2020)** 10432 – 10452, doi: 10.20964/2020.10.13

International Journal of ELECTROCHEMICAL SCIENCE
www.electrochemsci.org

Preparation of Ni–P–SiC composite coatings by magnetic field-enhanced jet electrodeposition

Feixiang Wang[1], *Xiuqing Fu*[1,2,*], *Moqi Shen*[1], *Ye XU*[1], *Shuanglu Duan*[1], *Qingqing Wang*[1], *Hongbing Cao*[1] *and Jinran Lin*[1]

[1] College of Engineering, Nanjing Agricultural University, Nanjing 210031, P. R. China;
[2] Key laboratory of Intelligence Agricultural Equipment of Jiangsu Province, Nanjing 210031, P. R. China
[*]E-mail: fuxiuqing@njau.edu.cn

Received: 8 June 2020 / *Accepted:* 31 July 2020 / *Published:* 31 August 2020

To explore the effect of magnetic field on the properties of Ni–P–SiC composite coatings, Ni–P–SiC composite coatings were prepared on 45 steel by magnetic field-enhanced jet electrodeposition. The surface morphology, microstructure, and composition of the composite coatings were measured by scanning electron microscopy (SEM), energy dispersive spectrometry (EDS), and X-ray diffraction (XRD), respectively. The microhardness was tested using a Duramin-40 hardness tester, and the corrosion resistance was observed under a LEXT4100 laser confocal microscope. The results showed that the surface of the Ni–P–SiC coatings prepared under a magnetic field-enhanced jet electrodeposition was flat. Moreover, we noted improvements in the microhardness, wear resistance, and corrosion resistance of the composite coatings with the increase in the magnetic field strength. At the same magnetic flux density, applying a parallel magnetic field was found to be more effective than applying a vertical magnetic field. When the parallel magnetic field intensity was 0.5 T, the coating surface was uniform and compact, and its microhardness reached the maximum value of 688.8 Hv, with optimal wear and corrosion resistances.

Keywords: Magnetic field; Jet electrodeposition; Ni–P–SiC coatings; Nano-SiC particles; Performance analysis

1. INTRODUCTION

Nano-SiC particles have a high oxidation resistance and stability [1,2]. Ni–SiC composite coatings can be prepared by co-depositing nano-SiC particles and Ni ions in a plating solution [3,4,5]. However, nano-SiC particles are prone to agglomeration and affect the coating performance. Currently,

studies on the agglomeration of nano-SiC particles are conducted in terms of plating solution parameters [6,7,8], current magnitude [9,10,11], stirring method [12-15], rotating composite electrodeposition [16], and magnetic field-enhanced electrodeposition [17,18].

The magnetic field-enhanced electrodeposition process has been widely studied in recent years. The magnetic field is a vector field that is continuously distributed in a certain spatial area. Its energy density is high and easy to control. It can transfer energy to the target material in a non-contact manner and will not cause any pollution or damage to the material. With the application of the conventional electrodeposition technology and combined with the magnetic field characteristics, the performance of a coating can be improved owing to the effects of the electric and flow fields generated during electrodeposition, namely improvements in the mass transfer process in the deposition process [19,26], surface conversion [20-22], physical and chemical properties of the plating solution, and other processes [23-27]. Currently, researchers are focusing on the magnetic field-enhanced technology through electrodeposition experiments. The scope of existing studies has been limited to either changing the magnetic flux density or the direction. Further, studies have shown that compared with conventional electrodeposition, jet-electrodeposition has a better effect on plating [28-30].

In this work, Ni–P–SiC composite coatings were prepared by magnetic field-enhanced jet electrodeposition under varying magnetic flux densities (0.2, 0.3, 0.4, and 0.5 T). The effects of magnetic field application, magnetic flux density, and direction on the surface morphology and performance of the composite coatings prepared by conventional jet electrodeposition were discussed. Finally, the wear and corrosion resistances of the composite coatings were analyzed.

2. MATERIALS AND METHODS

2.1. Experimental device

Fig. 1a shows the jet electrodeposition system. As shown, a nickel rod is connected to the positive pole of the power supply and assembled in the nozzle on the machine tool spindle. The workpiece is installed on the workpiece installation platform below the nozzle. The workpiece installation platform is connected to the negative pole of the power supply. After the power is switched on, the nozzle reciprocates, and the anode nickel bar, plating solution, and cathode workpiece form a closed loop, thus realizing ion deposition.

Fig. 1b shows the parallel magnetic field-enhanced jet electrodeposition system. The magnetic platform, made of NdFeB, is installed on the workpiece mounting platform, providing a stable parallel magnetic field. Fig. 1c shows the vertical magnetic field-enhanced jet electrodeposition system. Here, the magnetic platform, made of NdFeB, is installed on both sides of the workpiece installation platform to provide a stable vertical magnetic field.

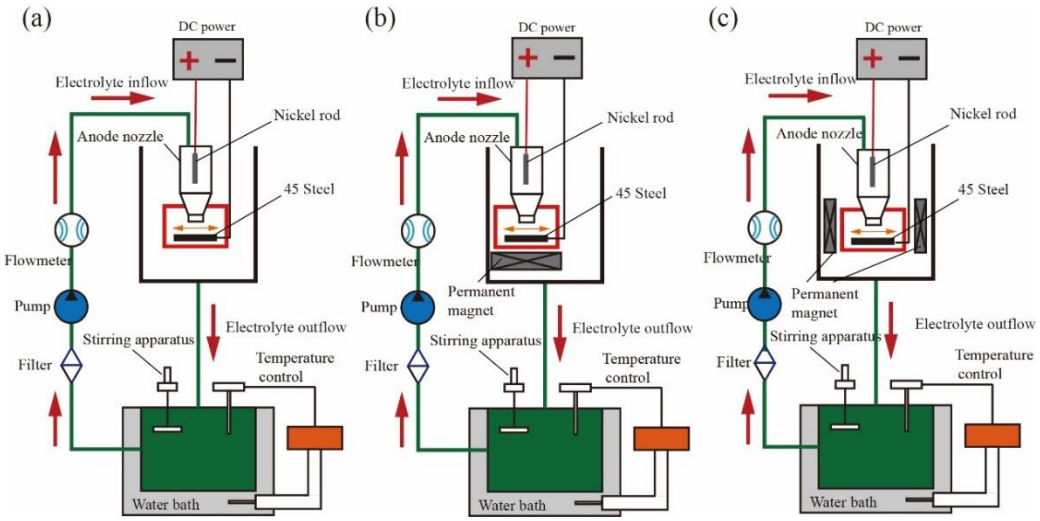

Figure 1. Schematics of Ni–P–SiC composite coating preparation: (a) Conventional jet electrodeposition, (b) Parallel magnetic field-enhanced jet electrodeposition, (c) Vertical magnetic field-enhanced jet electrodeposition system

2.2. Experimental content and parameters

The base material was a A#45 workpiece steel (25 mm × 10 mm × 8 mm), sanded with 320#, 800#, and 2000# sandpaper until a reflective surface appeared (Ra ≤ 0.1). The workpiece was placed in anhydrous ethanol for ultrasonic cleaning.

Table 1. Plating solution composition and processing conditions.

Chemical reagent	Content ($g \cdot L^{-1}$)
$NiSO_4 \cdot 6H_2O$	200
$NiCl_2 \cdot 6H_2O$	30
H_3PO_3	20
H_3BO_3	30
$C_6H_8O_7$	60
CH_4N_2S	0.01
$C_{12}H_{25}SO_4Na$	0.08
SiC (40 nm)	3
Electrodeposition parameters	**Amount**
Temperature (℃)	60±1.0
pH	1.0–1.5
Plating time (min)	25
Anode–cathode distance (mm)	1.5
Magnetic flux density (T)	0.2, 0.3, 0.4, 0.5
Plating current (A)	0.8

Based on preliminary experimental analyses [5,31], the following operating parameters are employed for basic experimental research on the preparation of Ni–P–SiC composite coatings by magnetic field-enhanced jet electrodeposition: a plating current of 0.8 A, a bath temperature of 60 ℃, a processing time of 25 min, and a bath flow rate of 4.5 m/s. Table 1 lists the composition and content of the bath. The magnetic platform provides a stable magnetic field (0.2, 0.3, 0.4, and 0.5 T). Before jet electrodeposition, the workpiece was pretreated as follows: Electric deoiling → Weak activation → Strong activation. The size of the nano-SiC particles was 40 nm. To evenly distribute the nano-SiC particles in the plating solution, the plating solution was magnetically stirred (5 h) to reduce the agglomeration force. The workpiece was cleaned and dried by ultrasonic waves after processing.

2.3. Test instrument

A Quanta FEG250 scanning electron microscope (FEI Instruments, Oregon, USA) was employed to observe the surface morphology of the prepared coating, at an acceleration voltage of 15 kV and a scanning rate of 30 μs. The XFlash 5030 EDS spectrum analyzer (Bruker AXS, Berlin, Germany) was used to determine the elements and their contents in the composite coating, at an acceleration voltage of 16 kV and a scanning area of 1 mm^2. The PANalytical X'pert X-ray diffractometer was used to analyze the phase structure composition of the coating; the working voltage was 40 kV, the scan rate was 5 $°min^{-1}$, and the scan range was 10–100°. The HighScore Plus software was used to analyze the XRD results. The Duramin-40 digital microhardness tester was used to measure the microhardness of the composite coating; the load was 100 g, the load loading time was 15 s, and five values were measured on each workpiece, and the average value was taken. The material surface performance comprehensive tester CFT-I was used for friction and wear tests. During the detection, a GCr15 grinding ball with a diameter of 5 mm was used to scratch the coating surface for 20 min; the scratch length was 4 mm, and the load was 320 g. An OLYMPUS LEXT4100 laser confocal microscope (Olympus Corporation, Japan) was used to image and measure the dimensional parameters of the coating surface scratches. The computations were made on an electrochemical workstation CS350 produced by Wuhan Corrtest Instruments Co. Under open circuit potential, the polarization curve and impedance spectrum were obtained using dynamic potential scanning and AC impedance method. The test workpiece was immersed in a 3.5 wt.% NaCl solution, and the polarization curve of the coating was obtained using the dynamic potential scanning method (at a scan rate of 1 mV/s). Subsequently, the parameters of the corrosion resistors, namely the self-corrosion potential and self-corrosion current, were obtained using the epitaxial method. The AC impedance method (EIS) was used to measure the impedance spectrum of the coating in the corrosive medium at the open circuit potential. The test frequency range was 10^{-2}–10^{-5} Hz, swept from high frequency to low frequency. The ZSimpWin software was used to fit and analyze the obtained impedance spectrum.

2.4. Analysis

In this work, the effects of magnetic field on the properties of the Ni–P–SiC coatings were studied. The effects of magnetic field application and varying magnetic field direction and magnetic

field intensity on the comprehensive properties of the coating were discussed. In the preparation of coatings, the Ni ions in the plating solution were absorbed firmly owing to the large specific surface area of the nano-SiC particles. Under the action of the electric field force, the nano-SiC particles were coated by the Ni ions and moved toward the cathode surface. The Ni ions gained electrons on the cathode surface and transformed into Ni atoms, forming a compact Ni–P–SiC composite coating. Therefore, we studied the effect of magnetic field coating performance by analyzing the effect of magnetic field on the Ni ions.

After the magnetic field is applied, it induces a Lorentz force (F_B) on the charged Ni ions in the bath during jet electrodeposition. To compare the Lorentz force (F_B) and electric field force (F_E) of the Ni ions during jet electrodeposition, we calculated F_B and F_E under magnetic fields applied in directions parallel and vertical to the electric field.

$$F_E = q.E \quad (1)$$

$$F_B = q.\upsilon.B.\sin\alpha \quad (2)$$

where q is the charge quantity of the Ni ions; E is the electric field intensity; υ is the velocity of the Ni ions; B is the magnetic field strength; α is the angle between the velocity direction of the Ni ions and the magnetic field.

Through calculations, we found that the Lorentz force and the electric field force are of the same magnitude, proving that the Lorentz force can change the movement trajectory of the Ni ions.

Fig. 2 shows the schematic of the Ni-ion trajectory and the stress acting on the cathode surface when preparing the Ni–P–SiC composite coatings.

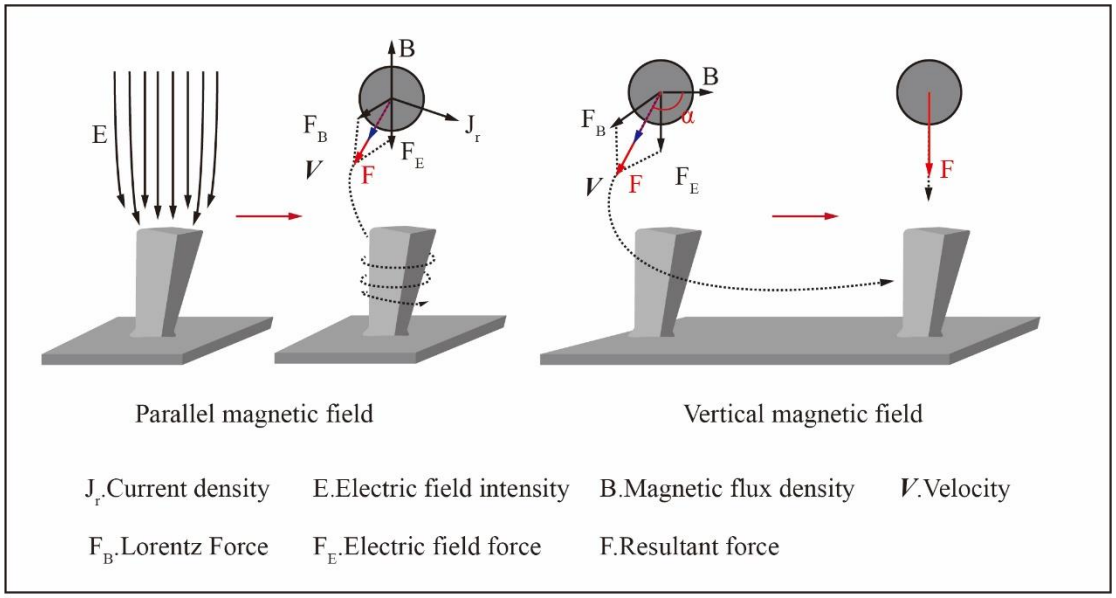

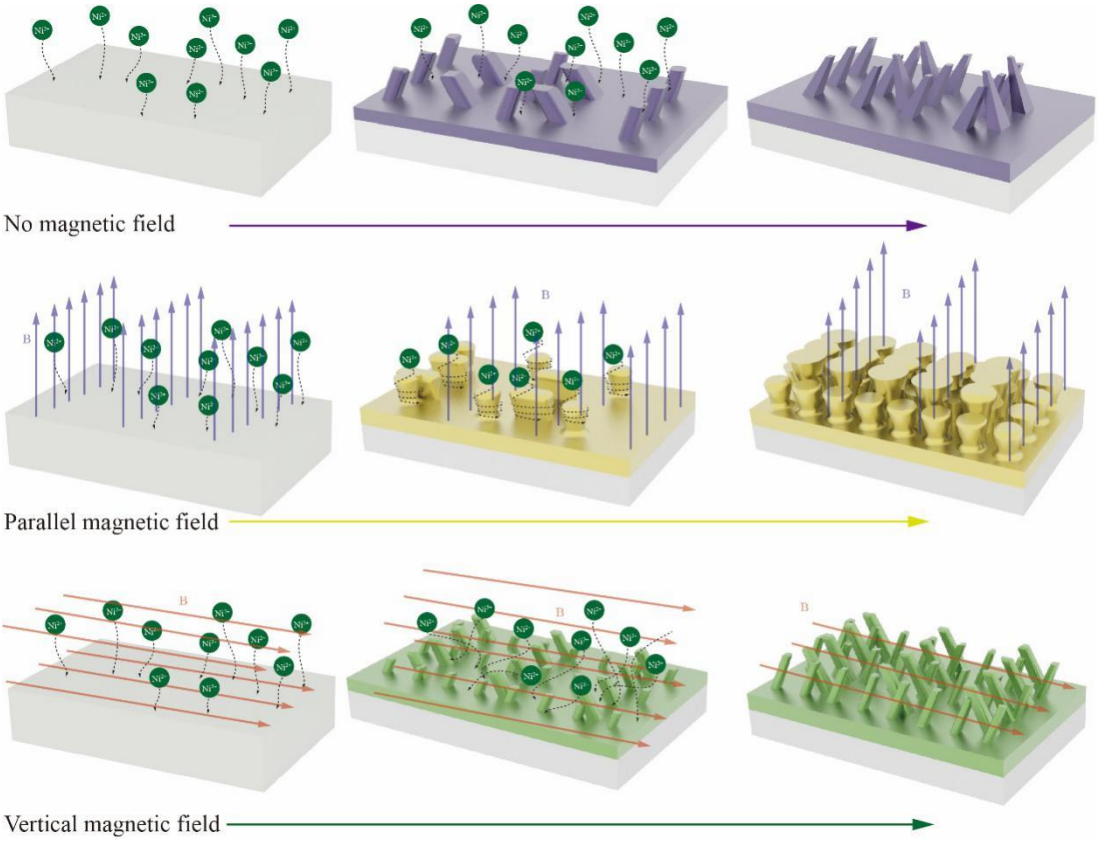

Figure 2. Mechanism of Ni ion jet electrodeposition under magnetic fields applied in directions vertical and parallel to the current direction.

In the conventional jet electrodeposition preparation process, Ni ions are directly impacted by the force of the electric field and fall directly into the deposition points. After the parallel magnetic field is applied, because the cathode surface is not ideally flat, electric field components are produced near the protrusion and deposition products during the deposition process. This leads to the generation of a micro-magnetohydrodynamics (MHD) effect on the surface of the cathode, where a tiny vortex appears at the front end of the grain, and the Ni ions wrap the nano-SiC particles rotating about the core or deposit under the action of the Lorentz and electric field forces, following the spiral diffusion path. Under the vertical magnetic field, the Ni ions are under the influence of a macro-magnetohydrodynamics (MHD) effect, and diffuse along the surface of the workpiece under the influence of the Lorentz force. When the Ni ions are close to the cathode surface, the Lorentz force is reduced because of the decrease in the angle between the velocity and the magnetic field. Finally, the Ni ions fall into the deposition points.

3. RESULTS AND DISCUSSION

3.1. Surface morphologies

Fig. 3 shows the surface morphology of the Ni–P–SiC coating prepared by conventional jet electrodeposition. As shown, the coating surface presents a typical cellular structure. This is because under the influence of the electric field force, Ni and P are adsorbed on the cathode surface, induced by

a catalytic surfactant, to deposit and form a solid solution. Their growth follows the 2D crystal core growth model [32]. The cell structure on the coating surface is evident. The boundary between the cell bodies is dense, and there are evident pits, processes, holes, and cracks. The flatness is poor as well. This is because during the deposition process, the reaction of hydrogen evolution on the cathode surface is violent, and the cells grow quickly [33].

Fig. 4 shows the surface morphology of the Ni–P–SiC composite coating prepared under a vertical magnetic field. When the vertical magnetic field is applied during the jet electrodeposition process (Figs. 4a, 4b, 4c, and 4d), the surface morphology of the composite coating varies significantly. The cellular structure becomes uniform, and the surface flatness is improved. Bund et al. [34] studied the magnetic field effects in electrochemical reactions, and found that the self-movement of ions increases under the effects of electric and magnetic fields, thus improving ion transmission in the plating solution and facilitating the formation of evenly dense coatings. In this study, the vertical magnetic field produced a macro-magnetohydrodynamics (MHD) effect on the coatings, which improved the Ni-ion transmission rate and the mass transfer efficiency near the electrode, resulting in reduced polarization on the cathode surface and improved uniformity of the Ni-ion distribution.

With the increase in the flux density of the vertical magnetic field, the surface quality of the composite coating is improved significantly. The coating surface is smoother, the cellular structure is tightly arranged, and the boundary is fuzzy. The number of defects, such as pits, is reduced. This is because the Lorentz force increases with the increase in the magnetic flux density [35], thereby increasing the speed of the Ni ions and the dispersion performance of the plating solution, enhancing the disturbance effect on the processing area, and reducing the surface concentration [36,37].

Fig. 5 shows the surface morphology of the Ni–P–SiC composite coating prepared under a parallel magnetic field. When a parallel magnetic field is applied during the jet electrodeposition process (Figs. 5a, 5b, 5c, and 5d), the cellular structure of the coating surface becomes flatter, and the surface flatness is further improved. Moreover, defects, such as pits and humps, are fewer, and the intercellular boundary is blurred. With increasing intensity of the parallel magnetic field, the surface roughness of the coating further decreases. When the magnetic flux density reaches 0.5 T, the tissues exhibit the best uniformity, and the surface topography is the smoothest. Morimoto et al. [38] studied the microscopic electrodeposition theory in parallel magnetic fields and showed that under the action of the micro-magnetohydrodynamics (MHD) effect, a vortex is generated on the cathode surface and that its intensity increases with the increase in the magnetic flux density. In this study, the vortex produced a scour effect, which hindered the growth of "needle" protrusions and flattened the protrusion front [39]. At the middle of the vortex, the flow velocity is relatively low, so the nano-particles tend to accumulate at the middle of the protrusions. The coating can well cover the nanoparticles, making each cellular structure more uniform.

At the same magnetic flux density, the coating prepared under the parallel magnetic field has better flatness, fewer defects, and more uniform cellular structure than that prepared under the vertical magnetic field. Compared with the macro-magnetohydrodynamics (MHD) effect, more nano-SiC particles are wrapped by the Ni ions and adsorbed on the cathode surface to form new nucleation points, making the coating surface smoother. The nano-SiC particles adsorb the Ni ions rotating about the core or deposit to form a flat, uniform-sized cellular structure.

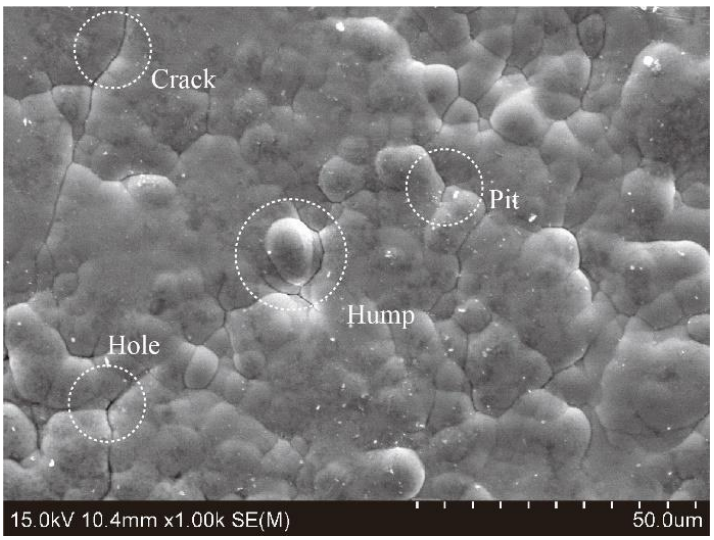

Figure 3. Surface morphology of the Ni–P–SiC composite coating prepared by conventional jet electrodeposition

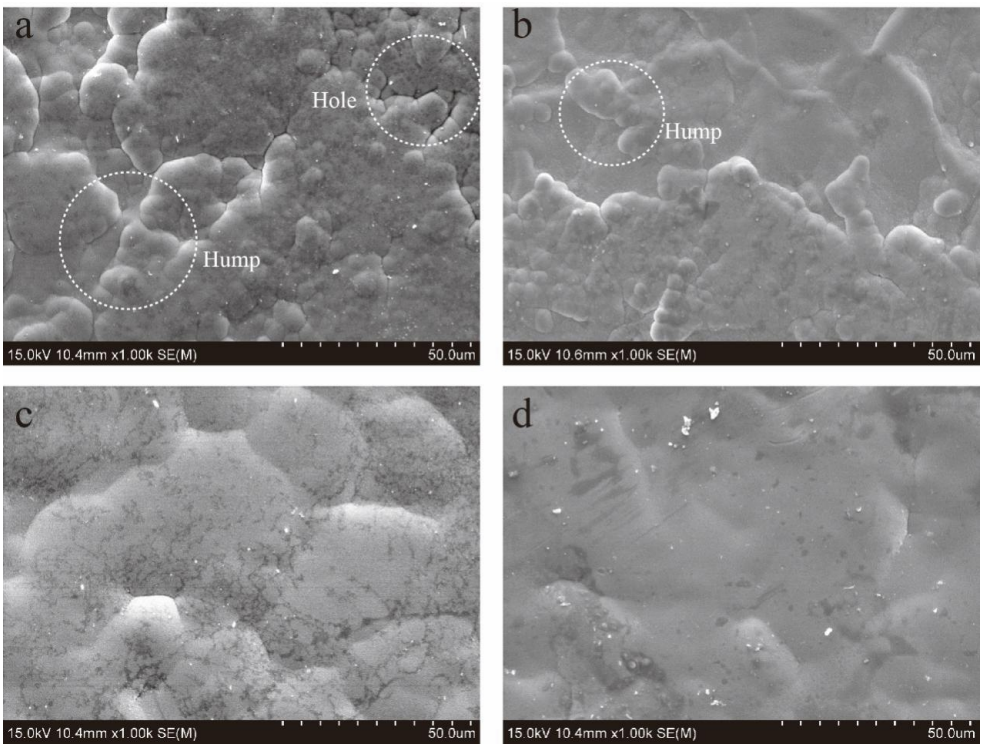

Figure 4. Surface morphologies of the Ni–P–SiC composite coating prepared by magnetic field-enhanced jet electrodeposition under varying vertical magnetic fields: a) 0.2 T, b) 0.3 T, c) 0.4 T, and d) 0.5 T.

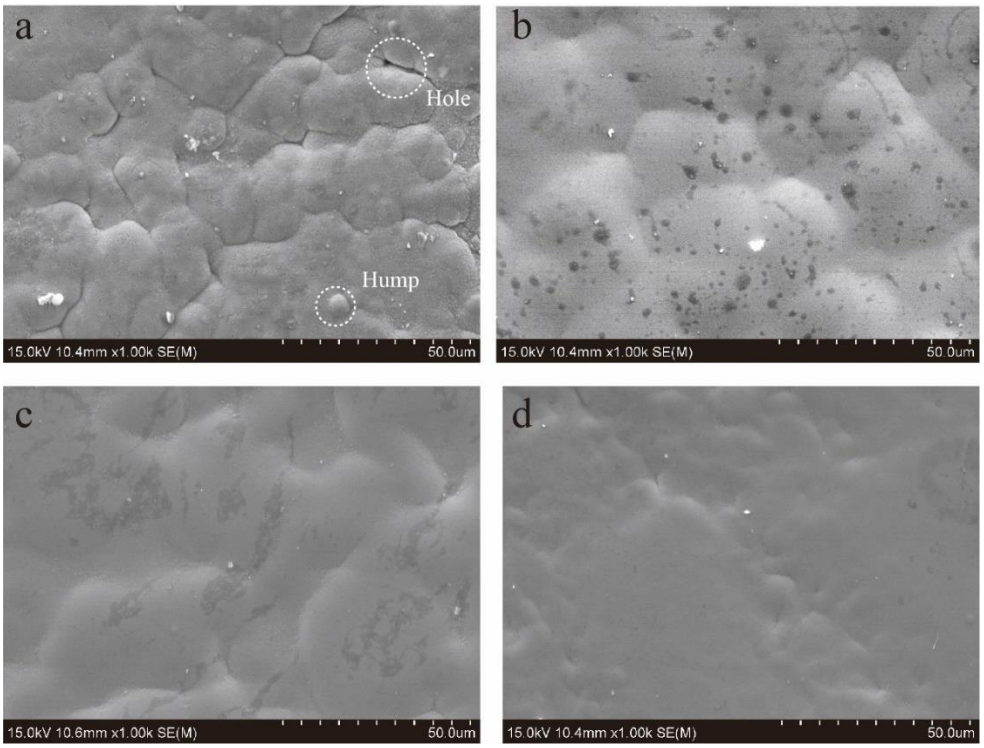

Figure 5. Surface morphologies of Ni–P–SiC composite coating prepared by magnetic field-enhanced jet electrodeposition under varying parallel magnetic fields: a) 0.2 T, b) 0.3 T, c) 0.4 T, and d) 0.5 T.

3.2. SiC contents

Fig. 6 shows the EDS analysis results of the Ni–P–SiC composite coatings. Based on the element compositions of the coating, Si is the only element related to the nano-SiC particles. Therefore, the Si element fraction was considered as the content of the nano-SiC particles in the coating. The Si element fraction of the Ni–P–SiC composite coating prepared by conventional jet electrodeposition is 1.4%. After the vertical magnetic field is applied, the Si content of the coatings increases. This is because the vertical magnetic field induces a macro-magnetohydrodynamics (MHD) effect on the surface of the cathode, thus generating a slight disturbance in the processing area. This improves the diffusibility of the Ni ions, increases the number of collisions between the nano-SiC particles and the Ni ions, and effectively reduces the polymerization tendency of the nano-SiC particles in the electrodeposition process. According to Guglielmi's adsorption theory [40], there exist two processes—weak adsorption and strong adsorption—before the particles enter the coating. With the assistance of the vertical magnetic field, the nano-SiC particles in the weak adsorption process are more likely to adsorb the Ni ions uniformly diffused into the bath, and there is less agglomeration between the particles. Therefore, the number of nano-SiC particles on the cathode surface increases during the strong adsorption phase.

With the increase in the magnetic flux density, the Si element fraction of the coatings increases. When the magnetic flux density reaches 0.5 T, the Si element fraction of the composite coating is 5.225%. This is because, with increasing magnetic flux density, the Lorentz force experienced by the Ni ions gradually increases [41]. Sugiyama et al. [42] studied the mass transfer process by magneto-

convention under a heterogeneous vertical magnetic field and reported that an increase in the magnetic flux density intensifies the ion movement. In this study, with the increase in the magnetic flux density, the self-motion and kinetic energy of the Ni ions were enhanced, and there was a higher probability of attaching to the surface of the nano-SiC particles during the co-deposition. More Ni ions wrapped the nano-SiC particles and moved directionally to the surface of the workpiece. Therefore, the increase in the magnetic flux density improved the content of nano-SiC particles in the coatings.

At the same magnetic flux density, the Si element fraction of the coating prepared under the parallel magnetic field was higher than that of the coating prepared under the vertical magnetic field. This is because the Lorentz force acting on the Ni ions and nano-SiC particles is different in different magnetic field directions. Huang et al. [26] studied lithium electrodeposition mechanism under a magnetic field and reported that Li ions in different magnetic field directions exhibit significant differences in terms of their motion trajectory during the deposition. In this study, under the vertical magnetic field, the Lorentz force acting on the Ni ions decreased when the velocity of the Ni ions approached the direction of the magnetic field. This made the vertical magnetic field lose its ability to evenly distribute the Ni ions. Under the parallel magnetic field, the velocity of the Ni ions is not strictly parallel to the direction of the magnetic field. The nano-SiC particles are evenly wrapped by the Ni ions and move along a spiral trajectory under the action of the resultant force. This type of movement brings about a better dispersion effect. Therefore, under the action of the parallel magnetic field, the content of nano-SiC particles in the coating was higher, and the particle distribution was more uniform.

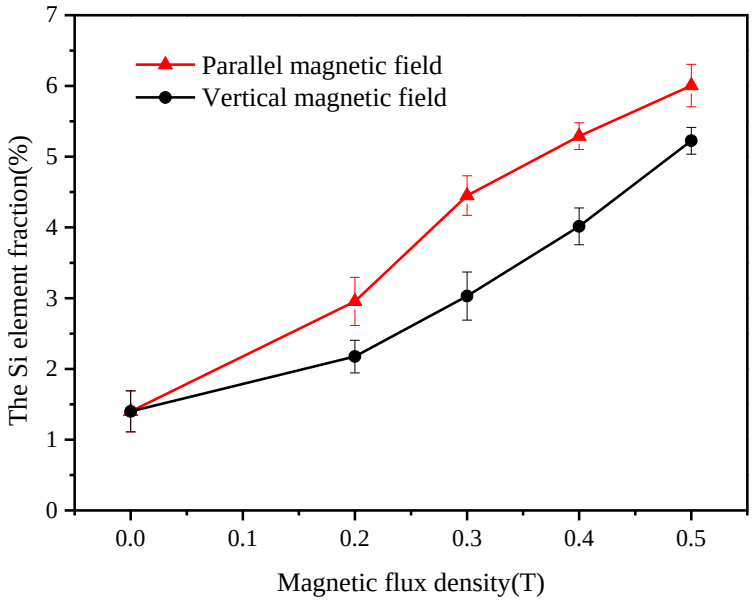

Figure 6. Relationship between magnetic flux density (0–0.5 T) and Si-element fraction of Ni–P–SiC composite coating.

When the magnetic flux density reaches 0.5 T, the Si-element fraction of the coating prepared under the parallel magnetic field reaches the maximum value of 6.005%. This is because with the increase in the magnetic flux density, the micro-magnetohydrodynamics (MHD) effect on the cathode surface is enhanced, and the eddy currents on the cathode surface are further enhanced. The Ni ions and

nano-SiC particles in the plating solution acquire higher kinetic energy, making them more likely to be "captured" by electrons on the workpiece surface. Thus, more Ni ions and nano-SiC particles co-deposit on the workpiece surface.

3.3. Phase constituent and crystallite size

Fig. 7a illustrates the effect of the magnetic flux density on the XRD pattern of the Ni–P–SiC composite coatings under the vertical magnetic field. The preferred orientation of the Ni–P–SiC composite coating is the (111) growth orientation, and the peak shapes at 2θ = 32°, 45°, 52°, 66°, and 83° are relatively sharp, and can be attributed to the characteristic XRD peaks for (110), (111), (200), (220), and (300) orientations, respectively. Fig. 7b shows the effect of magnetic field intensity on the XRD pattern of the Ni–P–SiC composite coatings under the parallel magnetic field. In the vicinity of 2θ = 45° and 52°, two wide diffusion dispersion peaks are found, which are the XRD characteristic peaks of (111) and (200), respectively, reflecting the characteristics of amorphous diffraction. As Ni is a transition group metal, and P is a metal-like element, there is a significant difference between their electronegativity, and the interaction force between the atoms is high, making it easy to form an amorphous state in the deposition process [43]. When the flux density of the parallel magnetic field is 0.2 T, the grain size of the Ni(111) element in the coating is 7.2 nm. With the increase in the magnetic field strength, the deposition rate of Ni and nano-SiC particles accelerates, the nucleation rate increases, and the grain size is further refined. When the flux density of the parallel magnetic field increases to 0.5 T, the grain size of the Ni(111) element in the coating reaches the minimum value of 4.8 nm. Based on the Hall–Petch relationship [44], as the diameter shrinks, the grains in the coating will be arranged more closely. A better coating performance can be obtained when the grains are closely arranged. By comparing the XRD patterns of the coatings prepared under the parallel and vertical magnetic fields, we find that with the increase in the parallel magnetic field, the (200), (220), and (300) crystal planes migrate to low-energy (111) and (200) crystal planes. Therefore, the performance of the coating prepared under the parallel magnetic field is more stable.

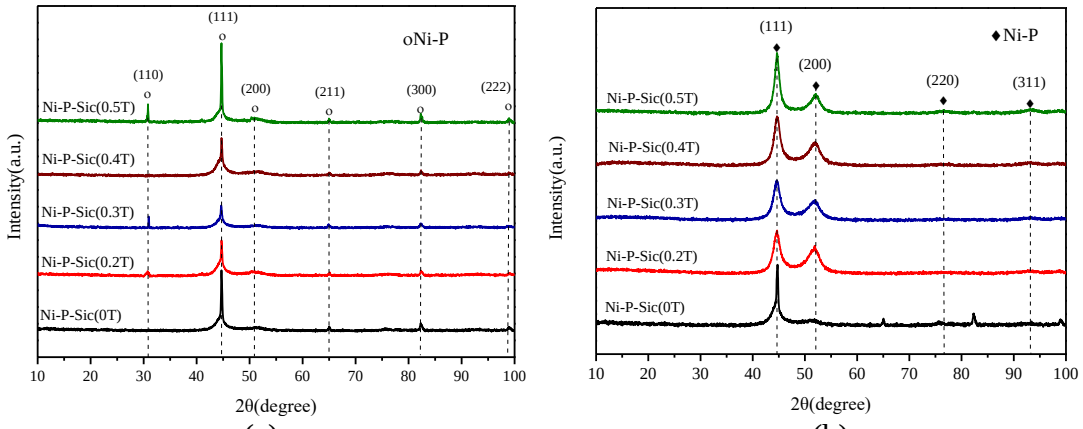

Figure 7. XRD patterns of Ni–P–SiC composite coatings prepared by field-enhanced jet electrodeposition under: (a) Vertical magnetic field, and (b) Parallel magnetic field.

3.4. Microhardness

Fig. 8 shows the microhardness of the Ni–P–SiC composite coating. The microhardness of the Ni–P–SiC composite coating prepared by conventional jet electrodeposition is 532.38 Hv. With the application of the vertical magnetic field, the microhardness of the coating increases significantly. In particular, with the increase in the flux density of the vertical magnetic field, the microhardness increases. When the magnetic flux density reaches 0.5 T, the microhardness reaches a maximum of 680.8 Hv. Ahmadkhaniha et al. [46] studied the influence of SiC particles on the micro-hardness of coatings and showed that one of the main reasons for the change in the microhardness is the diffusion strengthening of the second-phase hard particles in the coating. In our study, the content of nano-SiC particles in the coating increased after applying the vertical magnetic field. This improved the microhardness of the composite coating significantly.

The coating prepared under the parallel magnetic field exhibits a higher microhardness than that prepared under the vertical magnetic field. With increasing magnetic flux density, the microhardness of the composite coating increases. When the flux density of the parallel magnetic reaches 0.5 T, the microhardness of the composite coating reaches a maximum of 723.65 Hv. This is because the increase in the magnetic flux density enhances the magnetohydrodynamics (MHD) effect, thereby weakening the polymerization tendency of the nano-SiC particles in the plating solution. During the co-deposition process, the nano-SiC particles are more evenly dispersed. This facilitates the nano-SiC particles and Ni atoms to form a dense, hard, wear-resistant frame.

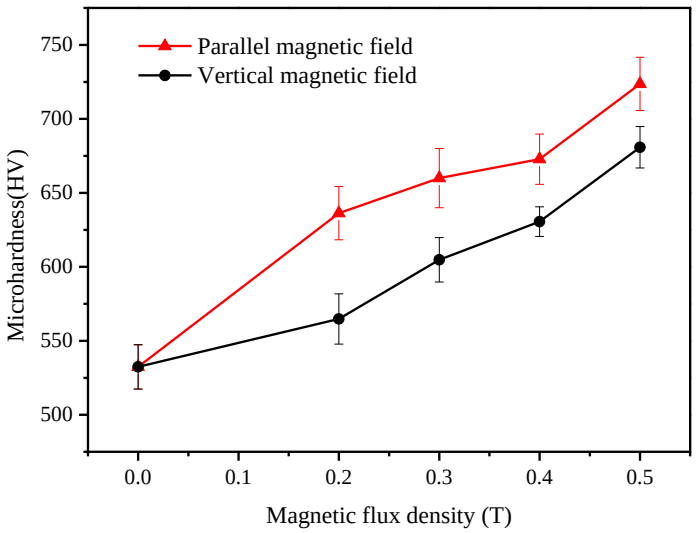

Figure 8. Microhardness of the Ni–P–SiC composite coating prepared by magnetic field-enhanced jet electrodeposition under varying magnetic flux density

3.5. Wear resistance analysis

The CFT-I material surface comprehensive performance tester was used to carry out friction and wear tests on the coating under normal temperature and no lubrication conditions. The wear resistance of the coating was compared and analyzed through the contour, and the parameters of the wear marks

were observed under the confocal microscope. Fig. 9 and Table 2 present the section morphology and parameters of the wear marks of the Ni–P–SiC composite coating, respectively.

The Ni–P–SiC coatings prepared by conventional jet electrodeposition exhibit the highest values of the wear mark width, depth, and cross-sectional area. The composite coating with the largest cross-sectional area exhibits the highest wear under the same wear scar length. According to the strength theory proposed by Mao- Yu et al. [46], the greater the plastic deformation, the more serious the adhesive wear of the coating. Therefore, the wear resistance of the coating was poor. When the vertical magnetic field was applied, the wear scar width, depth, and cross-sectional area of the coatings were reduced. With increasing flux density of the vertical magnetic field, the wear scar width, depth, and cross-sectional area of the coating generally exhibit a decreasing trend. Under the parallel magnetic field, the wear scar width, depth, and cross-sectional area of the composite coating are lower. With increasing magnetic flux density, the variations in the surface wear scar parameters of the coating exhibit a downward trend. When the magnetic flux density is 0.5 T, the wear scar width, depth, and cross-sectional area of the Ni–P–SiC composite coating reach minimum values: 321.505, 7.064, and 1193.680, respectively. The content of the nano-SiC particles in the Ni–P–SiC composite coating prepared by jet electrodeposition varies with the magnetic field strength and direction; thus, the composite coating has a dual performance of alloys and solid particles to some extent. With the increase in the content of nano-SiC particles, the adhesion area of the friction surface decreases, and the chimeric effect of the nano-SiC particles increases. The synergistic effect of the two significantly improves the coating wear resistance.

Fig. 9a shows the surface of the Ni–P–SiC composite coating prepared by conventional jet electrodeposition. Parallelly arranged plough furrows appear on the coating surface, and there are ridges and peeling scratches on the furrows. The coating is softened by frictional heat and produces a large plastic deformation. Some of the raised bonding points on the coating are sheared. The coating exhibits adhesive wear and partial shedding. The plastic deformation of the coating reaches its limit after being subjected to shear stress for a long time. Eventually, fatigue wear and spalling of the coating occur under all the applied loads [47]. This is because, in the conventional spray electrodeposition, the nano-SiC particles are unevenly distributed and cannot be dispersed effectively, so the strengthening effect of the nano-SiC particles on the coating is weak, and the abrasion resistance of the coating is moderate.

The wear scar morphologies of the Ni–P–SiC composite coating prepared by vertical magnetic field-enhanced jet electrodeposition are shown in Fig. 9b (0.2 T), Fig. 9d (0.3 T), Fig. 9f (0.4 T), and Fig. 9h (0.5 T). The peeling and plastic deformation of the coating are reduced. Chen et al. [48] studied the wear properties of Ni/TiN–SiC nanocoatings and showed that a high hardness of the nano-SiC particles can improve the wear resistance of the composite coatings. In this study, under the application of the vertical magnetic field, the content of nano-SiC particles in the coating increased significantly. The high hardness of the nano-SiC particles could help improve the wear resistance of the composite coatings. Moreover, the nano-SiC particles played a supporting role in the friction process of the coating and friction pair. Therefore, the wear condition of the plating layer was improved. Moreover, the wear form changed from adhesive wear to abrasive wear.

The wear scar morphologies of the Ni–P–SiC composite coating prepared by parallel magnetic field-enhanced jet electrodeposition are shown in Fig. 9c (0.2 T), Fig. 9e (0.3 T), Fig. 9g (0.4 T), and Fig. 9i (0.5 T). The wear condition of the coating prepared under the parallel magnetic field is much

better than that of the coating prepared under the vertical magnetic field. When the magnetic flux density reaches 0.5 T, the coating surface contains only minor scratches.

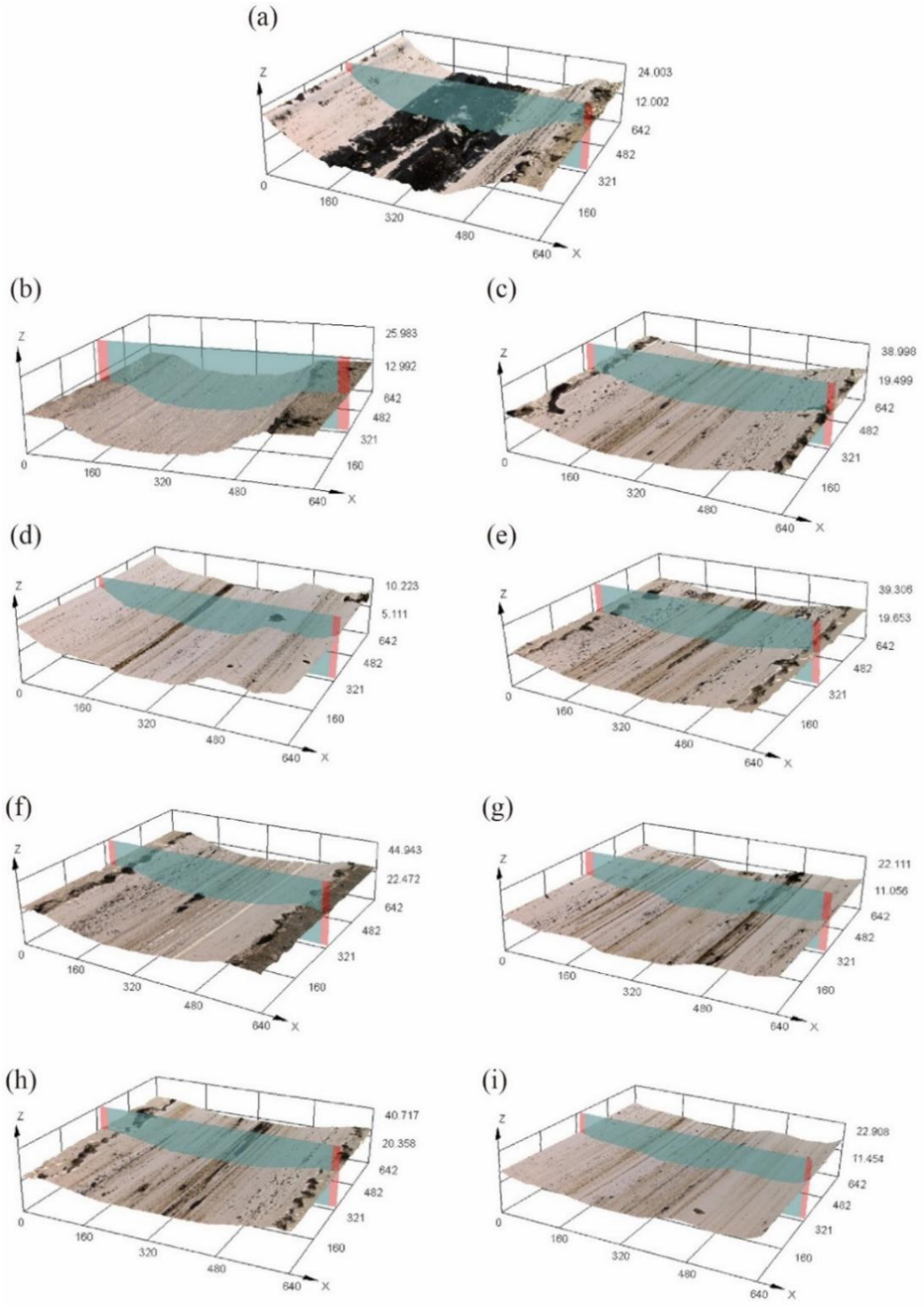

Figure 9. Outlines of the wear interfaces in: a) Ni–P–SiC coating (0 T) prepared by conventional jet electrodeposition; b) Ni–P–SiC coating (0.2 T), c) Ni–P–SiC coating (0.3 T), d) Ni–P–SiC coating (0.4 T), and e) Ni–P–SiC coating (0.5 T) prepared by vertical magnetic field-induced jet electrodeposition; f) Ni–P–SiC coating (0.2 T), g) Ni–P–SiC coating (0.3 T), h) Ni–P–SiC coating (0.4 T), and i) Ni–P–SiC coating (0.5 T) prepared by parallel magnetic field-induced jet electrodeposition.

The form of wear is abrasive wear. There are no evident furrows or flaking areas on the coating surface. This is because with the increase in the magnetic flux density, the micro-magnetohydrodynamics (MHD) effect increases, and the distribution of the nano-SiC particles in the coating becomes more uniform, forming a hard, wear-resistant frame. Therefore, the wear amount of the composite coating is low.

According to Archard's law [48], under the same experimental conditions, the wear resistance of a coating is proportional to its hardness. An increase in the microhardness is beneficial to improving the wear resistance of the coating. In this study, the application of a magnetic field helped improve the content of nano-SiC particles in the coating. The hardness of the coating was significantly improved owing to the dispersion strengthening and adhesion pinning of the nano-SiC particles, and the wear resistance of the coating was also enhanced.

Table 2. Parameters of wear mark section.

Magnetic field	Magnetic flux density (T)	Width (μm)	Height (μm)	Scratch area (μm^2)
No magnetic field	0	628.303	13.346	6258.331
Vertical magnetic field	0.2	549.682	11.173	5396.814
	0.3	496.711	9.788	3662.885
	0.4	436.422	7.856	2748.361
	0.5	395.049	7.183	1997.968
Parallel magnetic field	0.2	522.554	9.297	4114.131
	0.3	470.608	8.503	3525.173
	0.4	374.406	7.339	2429.689
	0.5	321.505	7.064	1193.680

3.6. Corrosion resistance

Fig. 10 shows the Tafel polarization curve of the Ni–P–SiC composite coating sample in the 3.5 g/L NaCl solution. The corrosion potential (E_{corr}) and corrosion current (i_{corr}) corresponding to the workpiece calculated using the Cview software and based on the polarization curve epitaxy method, respectively, are listed in Table 3. Generally, the lower the self-corrosion current density of a composite coating, the lower the corrosion rate; the greater the self-corrosion potential, the more difficult it is for the corrosion process to occur, and the better the corrosion resistance of the coating [49, 50]. As shown in Fig. 10a and Table 3, after the application of a vertical magnetic field, the corrosion potential shifts positively, the corrosion current density decreases, and the corrosion resistance of the coating is improved. With the increase in the intensity of the vertical magnetic field, the corrosion resistance of the coating continues to increase. From Fig. 10a, Fig. 10b, and Table 3, it can be found that under the parallel magnetic field, the corrosion potential corresponding to the coating is greater, and the corrosion current density is lower than that of the workpiece prepared under the vertical magnetic field. Moreover, the corrosion resistance of the coating increases with increasing magnetic flux density. The corrosion resistance is optimum at 0.5 T, the corrosion voltage (E_{corr}) is increased from −0.782 V (0 T) to −0.226 V (0.5 T), and the corrosion current (i_{corr}) is reduced from 9.56×10^{-5} A·cm^{-2} (0 T) to 2.92×10^{-6} A·cm^{-2}

(0.5 T). Evidently, the coatings prepared by the parallel magnetic field-enhanced jet electrodeposition exhibit a better corrosion resistance.

To further study the corrosion resistance of the Ni–P–SiC coatings, the AC impedance method (EIS) was used to measure the corrosion behavior of each sample in the 3.5 wt% NaCl solution. The Nyquist diagrams were plotted by measuring the impedance curves of the samples, as shown in Fig. 11. The results show that the capacitance impedance arc radius of the composite coating increases significantly with the application of the magnetic field. The coating prepared under the parallel magnetic field has a better corrosion resistance than that prepared under the vertical magnetic field. Among the prepared coatings, the capacitance impedance arc radius of the Ni–P–SiC (0.5 T) coating prepared with the assistance of the parallel magnetic field reaches the maximum. As a characterization of the electrochemical corrosion behavior of the coating, the higher the capacitance impedance arc radius, the higher the corrosion resistance of the coating [51,52]. To obtain sample corrosivity through a quantitative analysis, an equivalent circuit diagram model, as shown in Fig. 12, was proposed. The results were fitted using the ZSimpWin software, as listed in Table 4, where R_s is the resistance of the corrosion solution, R_p is the charge transfer resistance, and CPE is the constant-phase angle element. The impedance can be expressed as follows:

$$Z = \frac{1}{Y_0(j\omega)^{-n}} \quad (3)$$

where Y_0 has a dimension of $\Omega^{-1}\cdot cm^{-2}\cdot s^{-n}$, and the parameter n is a dimensionless index; if n = 0, the CPE element is a pure resistor; if n = 1, the CPE element is an ideal capacitor.

The equivalent resistance values were fitted using the EIS diagram and equivalent circuit (Table 4), and the results show that the application of the magnetic field significantly improves the corrosion resistance of the coatings and reduces the corrosion tendency of the sample. At the same magnetic flux density, the coatings prepared under the parallel magnetic field exhibit a higher charge transfer resistance than that prepared under the vertical magnetic field. When the magnetic flux density increases from 0 to 0.5 T, the charge transfer resistance (R_P) of the coatings is increased from 60 $\Omega\cdot cm^{-2}$ (0 T) to 820 $\Omega\cdot cm^{-2}$ (0.5 T).

In summary, applying the magnetic field during the preparation of the Ni–P–SiC composite coating by conventional jet electrodeposition can improve the corrosion resistance of the coating. With the increase in the magnetic flux density, the capacitance impedance arc radius of the coating increased. When the magnetic flux density increased to 0.5 T, the corrosion resistance of the composite coating was optimum. When the magnetic field was applied during the deposition process, the arrangement of the Ni atoms was more ordered, the self-movement of the nano-SiC nanoparticles intensified, and the polymerization tendency decreased. The atoms were closely arranged, the composite coating was denser, and the internal defects of the coating were reduced. The metal corrosion area exposed to the corrosive medium was effectively reduced. Therefore, the corrosion potential shifted positively, and the corrosion resistance of the coating was enhanced. When the magnetic field direction was parallel to the electric field, the arrangement of the Ni atoms and nano-SiC particles in the Ni–P–SiC composite coating was more uniform and dense. The coating protected the substrate better, and the corrosion resistance of the coating improved further.

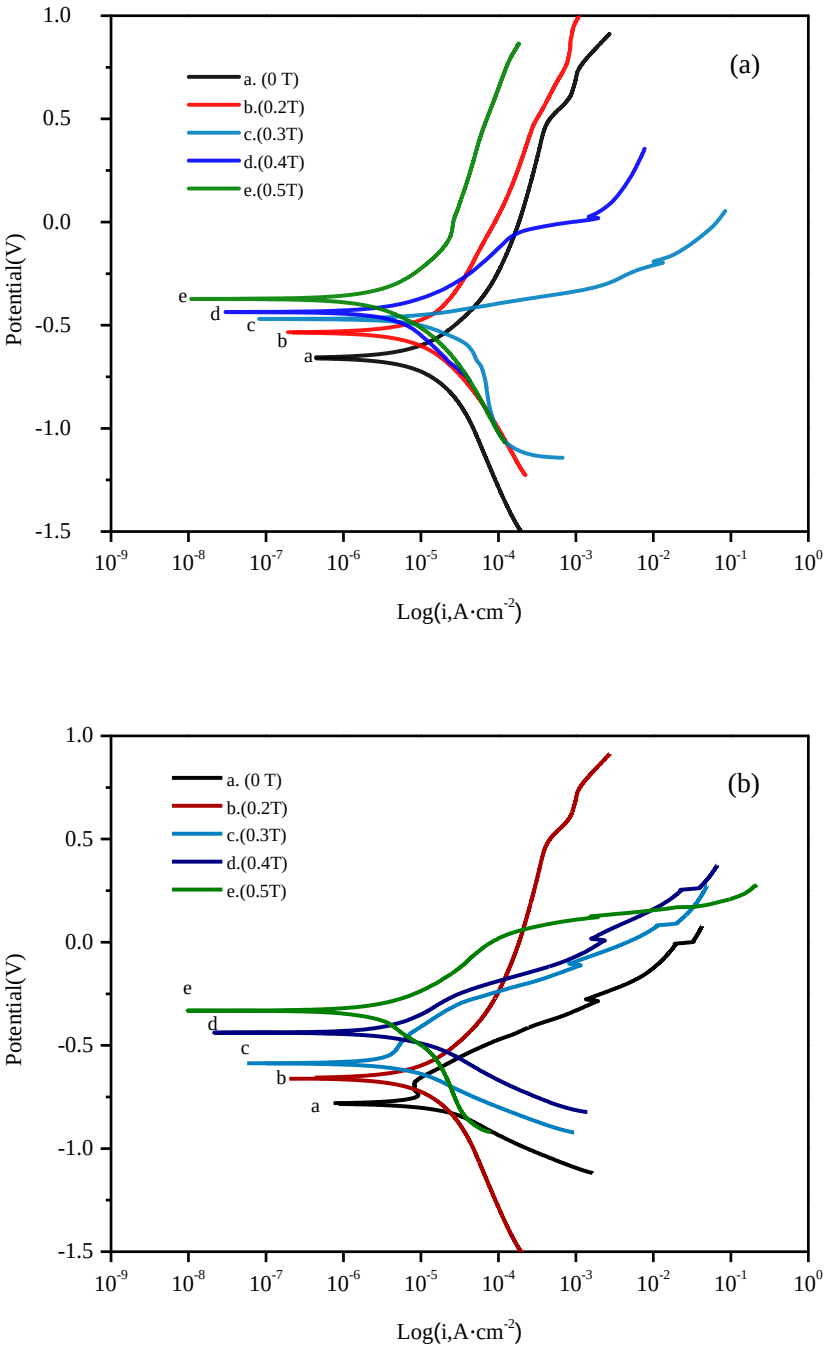

Figure 10. Potentiodynamic polarization curves of the Ni–P–SiC composite coating prepared by magnetic field-enhanced jet electrodeposition under: (a) Vertical magnetic field, (b) Parallel magnetic field

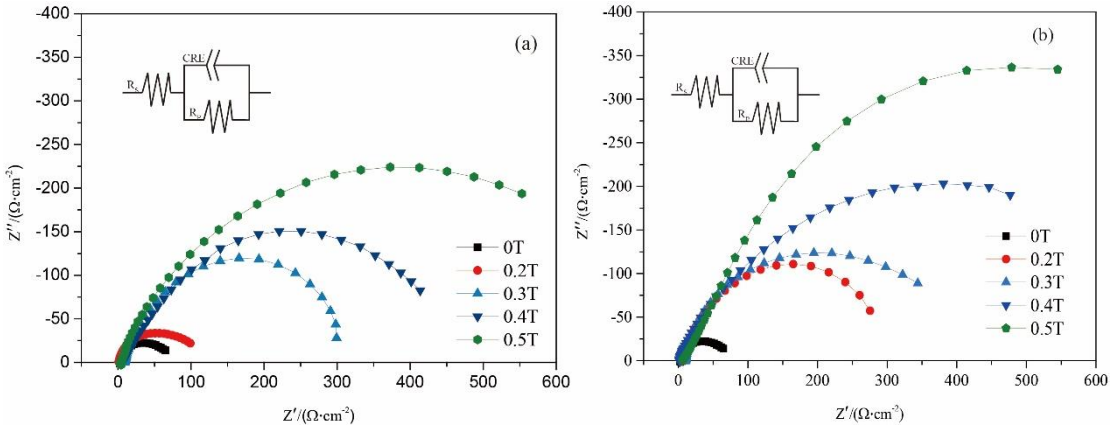

Figure 11. Nyquist plots of the Ni–P–SiC composite coating prepared by magnetic field-enhanced jet electrodeposition under: (a) Vertical magnetic field, (b) Parallel magnetic field

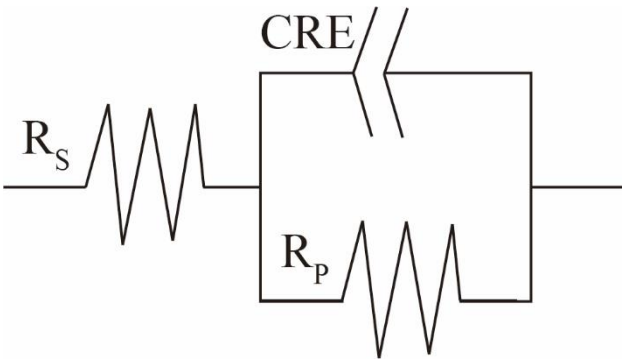

Figure 12. Equivalent circuit diagram model for Ni–P–SiC composite coatings

Table 3. Electrochemical and impedance data of the coatings

Magnetic field	Magnetic flux density (T)	E_{corr} (V)	i_{corr} (A·cm^{-2})
No magnetic field	0	−0.782	9.56×10^{-5}
Vertical magnetic field	0.2	−0.658	2.90×10^{-5}
	0.3	−0.587	6.01×10^{-6}
	0.4	−0.438	4.37×10^{-6}
	0.5	−0.331	3.56×10^{-6}
Parallel magnetic field	0.2	−0.535	1.43×10^{-5}
	0.3	−0.470	9.50×10^{-6}
	0.4	−0.436	6.99×10^{-6}
	0.5	−0.226	2.92×10^{-6}

Table 4. Fitted corrosion parameters for Ni–P–SiC composite coatings.

Magnetic field	Magnetic flux density (T)	R_S (Ω·cm^{-2})	CPE-T	CPE-P	R_P (Ω·cm^{-2})
No magnetic field	0	2.60	3.2917×10^{-2}	0.86	60
Vertical magnetic field	0.2	8.52	3.2753×10^{-3}	0.79	97
	0.3	8.63	6.8827×10^{-3}	0.82	215
	0.4	6.34	1.3719×10^{-3}	0.67	296

Parallel magnetic field	0.5	5.29	1.2232×10^{-3}	0.64	453
	0.2	5.92	2.3764×10^{-3}	0.58	187
	0.3	2.23	5.4285×10^{-3}	0.62	478
	0.4	4.12	8.4982×10^{-3}	0.70	675
	0.5	7.68	1.7218×10^{-3}	0.82	820

4. CONCLUSION

Ni–P–SiC composite coatings were prepared by jet electrodeposition technology. The effects of magnetic field application, magnetic flux density, and magnetic field direction on the microstructure, structure, and composition of the composite coatings were investigated, and the properties of the composite coatings were characterized. The following are the conclusions drawn from the results:

1) The Ni–P–SiC composite coating presented a typical cellular structure. Compared with the coating prepared by conventional jet electrodeposition, the surface roughness and surface quality of the coating prepared under a vertical magnetic field were better, and the coating quality improved with increasing magnetic flux density. At the same magnetic flux density, the surface of the coating prepared under the parallel magnetic field was flatter, and the cellular structure was more uniform than that prepared under the vertical magnetic field. When the flux density of the parallel magnetic field was 0.5 T, the surface density of the composite coating was the highest, the cellular structure was uniform, and the surface quality was the best.

2) The Ni–P–SiC composite coating exhibited an amorphous structure. Compared with the coating prepared by conventional jet electrodeposition, the Si element fraction of the coating prepared under the application of the magnetic field was higher. With the increase in the magnetic flux density, the Si element fraction continued to increase. Under the application of the parallel magnetic field, the Si element fraction in the coating was higher. When the flux density of the parallel magnetic field was 0.5 T, the Si element fraction of the composite coating reached the maximum value of 6.005%.

3) The dispersion strengthening effect of the SiC particles could significantly improve the microhardness of the Ni–P–SiC composite coating. Because the magnetohydrodynamics (MHD) effect generated by the magnetic field increased the content of nano-SiC particles in the composite coating, the distribution of the nano-SiC particles in the coating was more uniform. With the increase in the magnetic flux density, the magnetohydrodynamics (MHD) effect became more significant, and the microhardness of the coating was high. Due to the stronger diffusion of the Ni ions under the parallel magnetic field, the microhardness of the coatings was high. When the flux density of the parallel magnetic field was 0.5 T, the microhardness of the composite coating reached the maximum value of 723.65 Hv.

4) The width, depth, and cross-sectional area of the Ni–P–SiC composite coating decreased with increasing magnetic flux density. The coatings prepared by conventional jet-electrodeposition exhibited adhesive wear and serious wear. After the application of the magnetic field, the coating exhibited abrasive wear, and its wear resistance was significantly improved. Moreover, at the same magnetic flux density, the wear resistance of the coating prepared under the application of the parallel magnetic field was better than that of the coating prepared under the vertical magnetic field. When the flux density of the parallel magnetic field was 0.5 T, the wear resistance of the coating was the best.

5) Compared with conventional jet electrodeposition, the coatings prepared under the assistance of a magnetic field exhibited a higher corrosion potential, lower corrosion current, and greater equivalent impedance, representing an excellent corrosion resistance. With the increase in the magnetic flux density, the corrosion resistance of the coatings continuously improved, and became optimum when the flux density of the parallel magnetic was 0.5 T.

ACKNOWLEDGMENTS
This study was supported by the Fundamental Research Funds for the Central Universities (Grant number KYXJ202002), the China Postdoctoral Science Foundation (Grant number 2017M621665), the Postdoctoral Science Foundation of Jiangsu Province of China (Grant number 2018K022A), and the Innovation training for College students in Jiangsu Province of China (Grant number 202010307154Y).

References

1. W. Zhuo, L. D. Shen, M. B. Qiu, Z. J. Tian and W. Jiang, *Surf. Coat. Technol*., 333 (2018) 87.
2. F. F. Xia, W. C. Jia, C. Y. Ma and J. Wang, *Ceram. Int.*, 44 (2018) 766.
3. C. Wang, L. D. Shen, M. B. Qiu, Z. J. Tian and W. Jiang., *J. Alloys Compd.*, 727 (2017) 269.
4. M. Jiang, Z. X. Liu, L. J. Ding and J. J. Chen., *Catal. Commun.*, 96 (2017) 46.
5. X. Q. Fu, M. Q. Shen and J. R. Lin, *Int. J. Electrochem. Sci.*, 15 (2020) 816.
6. S. Dehgahi, R. Amini and M. Alizadeh, *J. Alloys Compd.*, 692 (2017) 692.
7. S. A. Ataie and A. Zakeri, *J. Alloys Compd.*, 674 (2016) 315.
8. I. Tudela, Y. Zhang, M. Pal, I. Kerr and A. J. Cobley, *Surf. Coat. Technol.*, 276 (2015) 89.
9. J.A. Calderón, J. E. Henao and M. A. Gómez, *Electrochim. Acta.*, 124 (2014) 190.
10. H. Ogihara, H. Wang and T. Saji, *Appl. Surf. Sci.*, 296 (2014)108.
11. A. Góral, M. Nowak, K. Berent and B. Kania, *J. Alloys Compd.*, 615 (2014) 406.
12. B. Bakhit and A. Akbari, *J. Alloys Compd.*, 560 (2013) 92.
13. D. G. Li, A. Levesque, A. Franczak, Q. Wang, J. C. He and J. P. Chopart, *Talanta*, 110 (2013) 66.
14. P. M Ming, Y. J. Li, S. Q. Wang, S. Z. Li and X. H. Li, *Surf. Coat. Technol.*, 213 (2012) 299.
15. H. Gül, F. Kılıç, M. Uysal, S. Aslan, A. Alp and H. Akbulut, *Appl. Surf. Sci.*, 258 (2012) 4260.
16. R. J. Sen, S. Das and K. Das, *Surf. Coat. Technol.*, 205 (2011) 3847.
17. M. Zieliński and E. Miękoś, *J. Appl. Electrochem.*, 38 (2008) 1771.
18. L. Benea, F. Wenger, P. Ponthiaux and J. P. Celis, *Wear*, 266 (2008) 398.
19. M. R. Vaezi, S. K. Sadrnezhaad and L. Nikzad, *Colloids Surf., A*, 315 (2008) 176.
20. P. F. Jiang, J. T. Wang, L. Hou, Y. Fautrelle and X. Li, *J. Mater. Sci. Technol.*, 50 (2020) 86.
21. S. S. Shuai, X. Lin, Y. H. Dong, L. Hou, H. L. Liao, J. Wang and Z. M. Ren, *J. Mater. Sci. Technol.*,35 (2019) 1587.
22. C. S. Li, S. D. Hu, Z. M. Ren, Y. Fautrelle and X. Li, *J. Mater. Sci. Technol.* 34 (2018) 2431.
23. Y. J. Li, Y. F. Teng, X. H. Feng and Y. S. Yang, *J. Mater. Sci. Technol.*, 33 (2017) 105.
24. B. Xu, W. P. Tong, C. Z. Liu, H. Zhang, L. Zuo and J. C. He, *J. Mater. Sci. Technol.*,27 (2011) 856.
25. J. Hu, C. F. Dong, X. G. Li and K. Xiao, *J. Mater. Sci. Technol.*, 26 (2010) 355.
26. Y. Q. Huang, X. S. Wu, L. Nie, S. J. Chen, Z. T. Sun, Y. J. He and W. Liu, *Solid State Ionics,* 345 (2020) 115171.
27. J. A. Koza, M. Uhlemann, C. Mickel, A. Gebert and L. Schultz, *Electrochim. Acta,*53 (2009) 5344.
28. F. F. Xia, Q. Li, C. Y. Ma and X. G., *Ceram. Int. ,*46 (2009) 2500.

29. L.D. Shen, W. Zhuo, M.B. Qiu, W. Jiang, K.L. Zhao and C. Wang, *Mater. Sci. Technol.*, 34 (2018) 419.
30. D. D. Ning, A. Zhang, M. Murtaza and H. Wu, *J. Alloys Compd.*, 777 (2019) 1245.
31. M. Q. Shen, X. Q. Fu, X. S. Wang, J. R. Lin and Q. Q. Wang, *Nanosci. Nanotechnol. Lett.*, 11 (2019) 938.
32. T. N. Qin, L. Q. Ma, Y. Yao, *Trans. Nonferrous Met. Soc. China*, 21 (2011) 2821.
33. X. T. Yu, M. Y. Wang, Z. Wang, X. Z. Gong and Z. C. Guo, *Appl. Surf. Sci.* ,360 (2016) 502.
34. A. Bund, S. Koehler, H. H. Kuehnlein and W. Plieth, *Electrochim. Acta*, 49 (2003) 147.
35. L. M. A. Monzon and J. M. D. Coey, *Electrochem. Commun.*, 42 (2014) 38.
36. C. Wang, Y. B. Zhong, W. L. Ren, Z. S. Lei, Z. M. Ren, J. Jia and A. R. Jiang, *Appl. Surf. Sci.*, 254 (2008) 5649.
37. W. Jiang, L. D. Shen, M. B. Qiu, X. Wang, M. Z. Fan and Z. J. Tian, *J. Alloys Compd.*, 762 (2018) 115.
38. R. Morimoto, M. Miura, A. Sugiyama, M. Miura and R. Aogaki, *J. Electroanal. Chem.*, 848 (2019) 113254.
39. P. Jin, C. F. Sun, Z.H. Zhang, C. Y. Zhou and T. Williams, *Surf. Coat. Technol.*, 392 (2020) 125738.
40. J. Tan, H. Song, X. H. Zheng, Q. Zhang and M. Wang, *Surf. Eng.*, 34 (2018) 861.
41. H. R. Ashorynejad and A. Zarghami, *Int. J. Heat Mass Transfer*, 119 (2018) 247.
42. A. Sugiyama, S. Morisaki and R. Aogaki, *Jpn. J. Appl. Phys.*, 42 (2003) 5322.
43. H. Sun, H.F. Ma and X. F. Guo, *J. Rare Earths*, 32 (2014) 228.
44. A. G. Sheinerman, R. H. R. Castro, M.Y. Gutkin, *Mater. Lett.*, 260 (2020) 126886.
45. Y. Yang and Y. F. Cheng, *Electrochim. Acta*, 109 (2013) 638.
46. D. Ahmadkhaniha, F. Eriksson, P. Leisner and C. Zanella, *J. Alloys Compd.*, 769 (2018) 1080.
47. M. H. Yu, V. A. Kolupaev, Y. M. Li and J. C. Li, *Procedia Eng.*, 10 (2011) 2508.
48. B. H. Chen, S. G. Liu, P. F. Ji, B. Li, X. Y. Zhang, M. Z. Ma and R. P. Liu, *J. Alloys Compd*., 831 (2020) 154839.
49. T. Telliskivi, *Wear*, 256 (2004) 817.
50. N. D. Ho, K.K. Moon, S.G. Hyeon, K.J. Hoon, L.C. Hun, L.S. Taek and A.H. Seon, *Int. J. Heat Mass Transfer*, 155 (2020) 119857.
51. R. Yi, Y. Zhang, X. Q. Zhang, F. Z. Fang, H. Deng, *Int. J. Mach. Tool. Manu.*, 150 (2020) 103517.
52. K. B. Deshpande, *Electrochim. Acta.*, 56 (2011) 1737.